Articles

2007

A Simple Sol-Gel Processing for the Development of High-Temperature Stable Photoactive Anatase Titania

Suresh Pillai
Technological University Dublin, suresh.pillai@tudublin.ie

Declan McCormack
Technological University Dublin, Declan.mccormack@tudublin.ie

John Colreavy
Technological University Dublin, john.colreavy@tudublin.ie

Recommended Citation

2007-01-01

A Simple Sol-Gel Processing for the Development of High-Temperature Stable Photoactive Anatase Titania

Suresh C. Pillai

Declan McCormack

John Colreavy

A Simple Sol−Gel Processing for the Development of High-Temperature Stable Photoactive Anatase Titania

Sibu C. Padmanabhan,[†] Suresh C. Pillai,*,[‡] John Colreavy,[‡] Sivakumar Balakrishnan,[†] Declan E. McCormack,[§] Tatiana S. Perova,[||] Yurii Gun'ko,[†] Steven J. Hinder,[⊥] and John M. Kelly[†]

School of Chemistry, Trinity College Dublin, Dublin 2, Ireland, Centre for Research in Engineering Surface Technology (CREST), FOCAS Institute, Dublin Institute of Technology, Camden Row, Dublin 8, Ireland, School of Chemical and Pharmaceutical Sciences, Dublin Institute of Technology, Kevin Street, Dublin 8, Ireland, Department of Electronic and Electrical Engineering, Trinity College Dublin, Dublin 2, Ireland, and The Surface Analysis Laboratory, School of Engineering, University of Surrey, Guildford, Surrey, GU2 7XH, United Kingdom

A method for the preparation of anatase TiO_2, which is stable to a temperature as high as 900 °C, without using any complex cationic dopants is presented. The synthetic procedure involves the reaction of titanium tetraisopropoxide (TTIP) with trifluoroacetic acid (TFA) followed by hydrolysis and sol−gel conversion to the xerogel and further calcination. The retention of the anatase phase to high temperatures can be attributed to the presence of small amounts of fluorine in the lattice, which is gradually removed between 500 and 900 °C as confirmed by X-ray photoelectron spectroscopy and Fourier transform infrared spectroscopic analysis. Samples prepared with a 1:16 TTIP/TFA composition calcined at 900 °C showed significantly higher photocatalytic activity compared to the *control* sample, standard commercial photocatalyst Degussa P25, and samples prepared using acetic acid and oxalic acid. The high-temperature anatase phase stability, determined by X-ray diffraction and Raman spectroscopy, coupled with its high crystallinity, microporosity, and minimal oxygen vacancy contributes to improved photocatalytic activity.

Introduction

Titania (TiO_2) is well-known for its applications in high-refractive optics,[1] oxide semiconductors,[2] oxygen sensors,[3] photovoltaics,[4] photocatalysis,[5] and pigments.[6] A particular interest is in the development of TiO_2 anatase coatings for self-cleaning and hygienic applications,[7] where it is expected that the anatase form of TiO_2 should be most effective.[8] A recent commercial application has shown the effectiveness of such a photoactive silver-doped titania coating.[9] However, as the processing temperature required for this material was 900 °C, this coating contained 8% anatase and 92% rutile. The anatase-to-rutile transformation in synthetic titania usually occurs at temperatures in the range of 600−700 °C.[10,11] Therefore, there is a need for procedures which will produce anatase-phase TiO_2 which is stable at 900 °C. This challenge has been met in some cases by the addition of cationic dopants.[12] Except for a few cases,[13] however, the photoactivity of the cation-doped TiO_2 is decreased due to

* Corresponding author. Tel.: +353 1 4027946. Fax: +353 1 4027941. E-mail: suresh.pillai@dit.ie.
† School of Chemistry, Trinity College Dublin.
‡ Crest, Dublin Institute of Technology.
§ School of Chemical and Pharmaceutical Sciences, Dublin Institute of Technology.
|| Department of Electronic and Electrical Engineering, Trinity College Dublin.
⊥ School of Engineering, University of Surrey.

(1) (a) Wang, X. D.; Neff, C.; Graugnard, E.; Ding, Y.; King, J. S.; Pranger, L. A.; Tannenbaum, R.; Wang, Z. L.; Summers, C. J. *Adv. Mater.* **2005**, *17*, 2103. (b) King, J. S.; Graugnard, E.; Summers, C. J. *Adv. Mater.* **2005**, *17*, 1010. (c) Prokes, S. M.; Gole, J. L.; Chen, X. B.; Burda, C.; Carlos, W. E. *Adv. Funct. Mater.* **2005**, *15*, 161.
(2) Hoffmann, M. R.; Martin, S. T.; Choi, W.; Bahnemann, D. W. *Chem. Rev.* **1995**, *95*, 69.
(3) (a) Watson, J.; Ihokura, K. *Mater. Res. Soc. Bull.* **1999**, *6*, 14 and articles thereof. Materials". (b) Zhu, Y.; Shi, J.; Zhang, Z.; Zhang, C.; Zhang, X. *Anal. Chem.* **2002**, *74*, 120. (c) Morris, D.; Egdell, R. G. *J. Mater. Chem.* **2001**, *11*, 3207.
(4) (a) O'Regan, B.; Gratzel, M. A. *Nature* **1991**, *353*, 737. (b) Park, N.-G.; van de Lagemaat, J.; Frank, A. J. *J. Phys. Chem. B* **2000**, *104*, 8989. (c) Ito, S.; Zakeeruddin, S. M.; Baker, R. H.; Liska, P.; Charvet, R.; Comte, P.; Nazeeruddin, M. K.; Péchy, P.; Takata, M.; Miura, H.; Uchida, S.; Grätzel, M. *Adv. Mater.* **2006**, *18*, 1202.
(5) (a) Seery, M. K.; George, R.; Floris, P.; Pillai, S. C. *J. Photochem. Photobiol., A* **2007**, *189*, 258. (b) Fujishima, A.; Honda, K. *Nature* **1972**, *238*, 37. (c) Yu, J. C.; Yu, J.; Ho, W.; Zhang, L. *Chem. Commun.* **2001**, 1942. (d) Linsebigler, A. L.; Lu, G.; Yates, J. T., Jr. *Chem. Rev.* **1995**, *95*, 735. (e) Zhang, Z. B.; Wang, C. C.; Zakaria, R.; Ying, J. Y. *J. Phys. Chem. B* **1998**, *102*, 10871. (f) Anpo, M.; Shima, T.; Kodama, S.; Kubokawa, Y. *J. Phys. Chem.* **1987**, *91*, 4305. (g) Fujishima, A.; Rao, T. N.; Tryk, D. A. *J. Photochem. Photobiol., C* **2000**, *1*, 1.

(6) (a) Feldmann, C. *Adv. Mater.* **2001**, *13*, 1301. (b) Feldmann, C.; Jungk, H. O. *Angew. Chem., Int. Ed.* **2001**, *40*, 359.
(7) (a) Wang, R.; Hashimoto, K.; Fujishima, A.; Chikuni, M.; Kojima, E.; Kitamura, A.; Shimohigoshi, M.; Watanabe, T. *Nature* **1997**, *388*, 431. (b) Hashimoto, K.; Irie, H.; Fujishima, A. *Jpn. J. Appl. Phys., Part 1* **2005**, *44*, 8269. (c) Zhang, X.-T.; Sato, O.; Taguchi, M.; Einaga, Y.; Murakami, T.; Fujishima, A. *Chem. Mater.* **2005**, *17*, 696.
(8) Kamat, P. V. *Chem. Rev.* **1993**, *93*, 267.
(9) Machida, M.; Norimoto, K.; Kimura, T. *J. Am. Ceram. Soc.* **2005**, *88*, 95.
(10) (a) Kumar, K. N. P.; Keizer, K.; Burggraaf, A. J.; Okubo, T.; nagamoto, H.; Morooka, S. *Nature* **1992**, *358*, 48. (b) Kumar, S. R.; Pillai, S. C.; Hareesh, U. S.; Mukundan, P.; Warrier, K. G. K. *Mater. Lett.* **2000**, *43*, 286. (c) Kumar, S. R.; Suresh, C.; Vasudevan, A. K.; Suja, N. R.; Mukundan, P.; Warrier, K. G. K. *Mater. Lett.* **1999**, *38*, 161.
(11) (a) Yin, S.; Aita, Y.; Komatsu, M.; Sato, T. *J. Eur. Ceram. Soc.* **2006**, *26*, 2735. (b) Gandhe, A. R.; Naik, S. P.; Fernades, J. B. *Micropor. Mesopor. Mater.* **2005**, *87*, 103. (c) Cheng, P.; Qiu, J.; Gu, M.; Shangguan, W. *Mater. Lett.* **2004**, *58*, 3751.

its thermal instability or an increase in charge carrier recombination centers.[14]

High crystallinity and suitable surface properties (accessible surface area, porosity, and pore volume) are the other key factors that contribute to the photocatalytic activity. A possible high temperature heat treatment may be useful to accomplish these features, provided the anatase phase is stable against heat treatment. In this context, the possibilities of sulfate-modified anatase TiO₂ systems have been explored.[15] Thus, Colon et al. have prepared a highly crystalline TiO₂ powder with good photocatalytic activity for the destruction of phenol at 700 °C by sulfating a hydrous titania gel.[15a] They attributed the activity to minimal crystal defects evolved after the elimination of sulfate species. Similarly, Zhang et al. extended the anatase phase stability of TiO₂ up to 600 °C (873 K) by adding a small amount of sulfate species into the hydrolysis product of TiCl₄.[15b] As part of a program to develop high-temperature stable photoactive titania materials, we have recently prepared a nitrogen-doped titania which was stable up to 800 °C.[16] All these reports, however, involve a precipitate route synthesis which cannot be used for making thin films by dip-coating or spin-coating techniques. A sol−gel route should, on the other hand, be more effective in terms of the homogeneity of the sol, which is advantageous over the other techniques, and both powders and coatings can be prepared by a one-step sol−gel process. Here, we report a simple and effective sol−gel method to synthesize high-temperature stable (900 °C), photoactive anatase TiO₂, which we believe should be useful in the preparation of smart coatings for ceramics in hygienic applications.

The preparation method involves the modification of a precursor, titanium tetraisopropoxide (TTIP), with trifluoroacetic acid (TFA) followed by hydrolysis, gelation, drying, and heat treatment to achieve nanosized TiO₂. High-temperature heat treatment facilitates the preparation of highly crystalline anatase TiO₂ with minimal oxygen vacancy concentration. Methylene blue (MB) degradation experiments under UV light (365 nm) show its high activity, which is better than that of the commercial TiO₂, Degussa P25. In order to compare and deduce the effectiveness of this preparative route, samples such as acetic acid (HOAc)-

modified TiO₂,[17] oxalic acid (OxA)-modified TiO₂,[18] and a *control* TiO₂ (prepared without any modifier) have also been produced by similar procedures. The factors influencing the photocatalytic activity are discussed.

Experimental Section

In a typical synthesis {to prepare a sol (Ti-16TFA) with 1:16:4 (molar ratio) TTIP/TFA/H₂O}, 2.5 mL of TTIP was added to 4.4 mL of a TFA solution in a glass beaker under stirring. Subsequently, 0.60 mL of Millipore water was added dropwise into the clear solution formed, and the beaker was sealed using a parafilm, and stirring was continued for a further 1 h. After 24 h of aging at room temperature (20 °C), the sol was dried at 90 °C in an air oven to obtain the gel. The gel was then calcined at different temperatures such as 300, 500, 600, 700, 800, 900, and 1000 °C at a heating rate of 5 °C per minute and held at these temperatures for 2 h (samples Ti-16TFA-300 to Ti-16TFA-1000). Sols with 1:1, 1:4, 1:8, 1:12, and 1:32 Ti/TFA ratios were also prepared and converted by a similar method to TiO₂ gels. Similar compositions of Ti/HOAc/H₂O samples were also prepared for comparison. Ti/OxA/H₂O samples were prepared by dissolving oxalic acid crystals in 125 mL of absolute ethanol before the addition of TTIP. A standard (*control*-TiO₂) was prepared by adding 0.60 mL of Millipore water to 2.5 mL of a TTIP solution under stirring.

Characterization Techniques. Powder XRD patterns were recorded with a Siemens D 500 X-ray diffractometer in the 2θ range 20−70° using Cu Kα radiation. The anatase content in the sample was estimated using the Spurr equation:

$$F_A = 100 - \left(\frac{1}{1 + 0.8[I_A(101)/I_R(110)]}\right)100 \qquad (1)$$

where F_A is the mass fraction of anatase in the sample and I_A and I_R are the integrated intensities of the main peaks of anatase (101) and rutile (110), respectively. Crystallite sizes were calculated from the peak widths using the Scherrer equation $\Phi = k\lambda/(\beta \cos \theta)$, where Φ is the crystallite size, k is the shape factor (a value of 0.9 was used in this study), λ is the X-ray radiation wavelength (1.546 Å for Cu Kα), and β is the line width at half-maximum height of the main intensity peak after subtraction of the equipment broadening. Room-temperature Raman spectra were recorded with a Renishaw 1000 micro-Raman system equipped with an Ar⁺ ion laser (Laser Physics Reliant 150 Select Multi-Line) with a typical laser power of ∼3 mW in order to avoid excessive heating. The 50×-magnifying objective of the Leica microscope focused the beam into a spot of about 1 μm in diameter. Fourier transform infrared spectroscopy (FTIR) spectra of the samples in KBr pellets were recorded using a Spectrum GX FTIR spectrometer in the range 4000−370 cm⁻¹. The BET specific surface area was measured using Nova Station A surface area analyzer (Quantachrome Instruments version 2.1). The pore size distribution was obtained using the Horvath−Kawazoe method.[19]

Diffuse reflectance spectra (DRS) of the samples were recorded using a Perkin-Elmer Lambda 900 UV/Vis/NIR spectrometer with an integrated sphere attachment. Sample pellets were prepared using

(12) (a) Choi, W.; Termin, A.; Hoffmann, M. R. *Angew. Chem.* **1994**, *106*, 1148. (b) Wang, C. Y.; Bahnemann, D. W.; Dohrmann, J. K. *Chem. Commun.* **2000**, 1539. (c) Choi, W.; Termin, A.; Hoffmann, M. R. *Angew. Chem., Int. Ed. Engl.* **1994**, *33*, 1091. (d) Liu, Y.; Liu, C. Y.; Rong, Q. H.; Zhang, Z. *Appl. Surf. Sci.* **2003**, *220*, 7. (e) Zhang, Y. H.; Zhang, H. X.; Xu, Y. X.; Wang, Y. G. *J. Mater. Chem.* **2003**, *13*, 2261. (f) He, J.; Ichinose, I.; Fujikawa, S.; Kunitake, T.; Nakao, A. *Chem. Mater.* **2002**, *14*, 3493.

(13) (a) Karakitsou, K. E.; Verykios, X. E. *J. Phys. Chem.* **1993**, *97*, 1184. (b) Yamashita, H.; Ichihashi, Y.; Takeuchi, M.; Kishiguchi, S.; Anpo, M. *J. Synchrotron Radiat.* **1999**, *6*, 451.

(14) (a) Choi, W.; Termin, A.; Hoffmann, M. R. *J. Phys. Chem.* **1994**, *98*, 13669. (b) Hermann. J. M.; Disdier, J.; Pichat, P. *Chem. Phys. Lett.* **1984**, *108*, 618.

(15) (a) Colon, G.; Hidalgo, M. C.; Navio, J. A. *Appl. Catal., B.* **2003**, *45*, 39. (b) Zhang, Q.; Gao, L.; Guo, J. *J. Eur. Ceram. Soc.* **2000**, *20*, 2153. (c) Yang, Q.; Xie, C.; Xu, Z.; Gao, Z.; Du, Y. *J. Phys. Chem. B* **2005**, *109*, 5554. (d) Bokhimi, X.; Morales, A.; Novaro, O.; Lopez, T.; Chimal, O.; Asomoza, M.; Gomez, R. *Chem. Mater.* **1997**, *9*, 2616.

(16) Pillai, S. C.; Periyat, P.; George, R.; McCormack, D. E.; Seery, M. K.; Hayden, H.; Colreavy, J.; Corr, D.; Hinder, S. J. *J. Phys. Chem. C* **2007**, *111*, 1605.

(17) (a) Sibu, C. P.; Kumar, S. R.; Mukundan, P.; Warrier, K. G. K. *Chem. Mater.* **2002**, *14*, 2876. (b) Suresh, C.; Biju, V.; Mukundan, P.; Warrier, K. G. K. *Polyhedron* **1998**, *17*, 3131.

(18) Bersani, D.; Antonioli, G.; Lottici, P. P.; Lopez, T. *J. Non-Cryst. Solids* **1998**, *232−234*, 175.

(19) (a) Horvath, G.; Kawazoe, K. *J. Chem. Eng. Jpn.* **1983**, *16*, 470. (b) Everett, D. H.; Powl, J. C. *J. Chem. Soc., Faraday Trans.* **1976**, *72*, 619. (c) Terzyk, A. P; Gauden, P. A. *Colloids Surf., A* **2001**, *177*, 57. (d) Roziere, J.; Brandhorst, M.; Dutartre, R.; Jacquin, M.; Jones, J. D.; Vatse, P.; Zajac, J. *J. Mater. Chem.* **2001**, *11*, 3264.

a 4 mm die after thoroughly mixing the powder samples with KBr.[20] The band gaps were calculated by extrapolating the lower wavelength cutoff region.
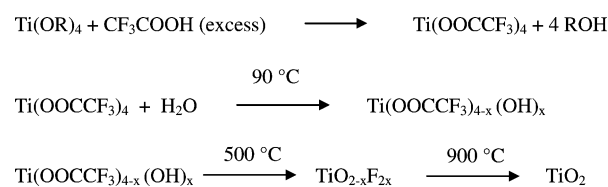
X-ray photoelectron spectroscopy (XPS) analyses were performed on a Thermo VG Scientific (East Grinstead, U.K.) Sigma Probe spectrometer. The instrument employs a monochromated Al Kα X-ray source ($h\nu$ = 1486.6 eV), which was used at 140 W. The area of analysis was approximately 500 μm in diameter for the samples analyzed. For survey spectra, a pass energy of 100 eV and a 0.4 eV step size were employed. For C_{1s} and Ti_{2p} high-resolution spectra, a pass energy of 20 eV and a 0.1 eV step size were used. For O_{1s} high-resolution spectra, a pass energy of 20 eV and a 0.2 eV step size were used. For F_{1s} and N_{1s} high-resolution spectra, a pass energy of 50 eV and a step size of 0.2 eV were used. Charge compensation was achieved by using a low-energy electron flood gun. Quantitative surface chemical analyses were calculated from the high-resolution core-level spectra, following the removal of a nonlinear Shirley background. The manufacturer's Avantage software was used, which incorporates the appropriate sensitivity factors and corrects for the electron energy analyzer transmission function.

Photoactivity Study. Photoactivity experiments were conducted by measuring the extent of degradation of an organic dye, methylene blue, in the presence of TiO_2. For this, 1.5 mg of TiO_2 powder was first dispersed in 4 mL of Millipore water in a UV cell. The suspension was then ultrasonicated for 10 min. A total of 0.1 mL of 2×10^{-3} M MB was then added to the suspension. The samples were irradiated under UV light using a Luzchem UV chamber (Canada) consisting of 10 8-W Hitachi-II tubes (wavelength 365 nm). The absorbance maximum of MB (664 nm) was measured after each interval of light irradiation from 0 min up to 85 min. The kinetics of the MB degradation were analyzed as reported previously.[5a,16] Photodegradation experiments had also been conducted in Irish sunlight on the 24th of July, 2006.

Results

The preparation method involves the reaction of TTIP with TFA followed by hydrolysis, gelation, drying at 90 °C, and heating (500−900 °C) to give nanosized TiO_2. The chemical sequence may be represented as shown in Scheme 1.

Scheme 1. Chemical Sequence of TFA Modified Sol−Gel Process

$$Ti(OR)_4 + CF_3COOH \text{ (excess)} \longrightarrow Ti(OOCCF_3)_4 + 4 \text{ ROH}$$

$$Ti(OOCCF_3)_4 + H_2O \xrightarrow{90\ °C} Ti(OOCCF_3)_{4-x}(OH)_x$$

$$Ti(OOCCF_3)_{4-x}(OH)_x \xrightarrow{500\ °C} TiO_{2-x}F_{2x} \xrightarrow{900\ °C} TiO_2$$

It is notable that, in contrast to the Ti-16HOAc system, where gelation occurs immediately upon the addition of water at room temperature (20 °C), the Ti-16TFA mixture (Supporting Information 1) does not gel, indicating that the rate of hydrolysis is considerably lower for the latter system. Indeed, this is further evident from the longer shelf life of the Ti-16TFA sol samples at room temperature (20 °C), and the xerogel is only formed upon heating to 90 °C. These materials have been found to be extremely robust in that they have remained stable in their prepared form for in excess of 1 year.

(20) Gauglitz, G.; Vo-Dinh, T. *Handbook of Spectroscopy*; Wiley-VCH: New York, 2003; Vol. 1, p 97.
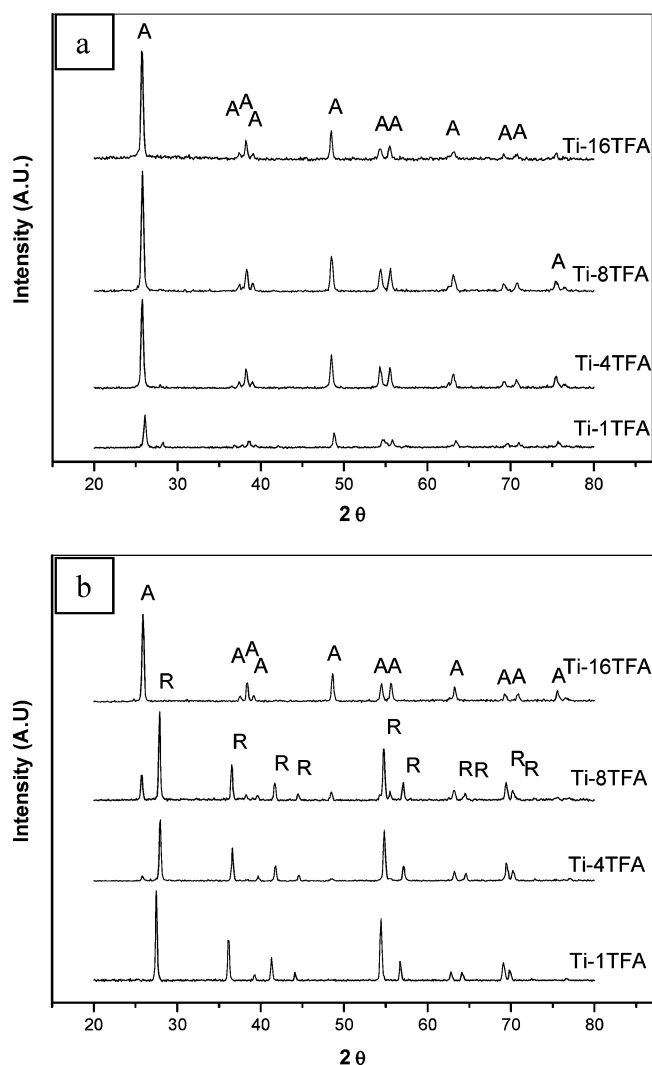

Figure 1. XRD patterns of various Ti-TFA samples (a) calcined at 700 °C and (b) calcined at 900 °C. (A, anatase; R, rutile).

Table 1. Crystalline Phases and Weight Percentages of Anatase and Rutile (A:R) Determined from XRD

sol used for preparation	% anatase (A):% rutile (R) at specified temperatures (error ± 5%)				
	600 °C	700 °C	800 °C	900 °C	1000 °C
Ti-32TFA	100:0	100:0	100:0	96:4	0:100
Ti-16TFA	100:0	100:0	100:0	100:0	0:100
Ti-12TFA	100:0	100:0	100:0	92:8	0:100
Ti-8TFA	100:0	100:0	90:10	43:57	0:100
Ti-4TFA	100:0	98:2	83:17	39:61	0:100
Ti-1TFA	100:0	82:18	25:75	0:100	0:100
Ti-16OxA	100:0	13:87	0:100	0:100	0:100
Ti-16HOAc	24:76	0:100	0:100	0:100	0:100
control TiO_2	18:82	0:100	0:100	0:100	0:100

X-ray Diffraction Analysis. The phase evolution of the samples has been followed by the powder X-ray diffraction (XRD) technique. The XRD patterns of the samples calcined at 700 and 900 °C are presented as Figure 1a and b, respectively. The percentage anatase and rutile contents calculated using the Spurr equation are presented in Table 1. It may be noted that a 100% anatase TiO_2 was observed at a temperature as high as 900 °C for the sample prepared from the Ti-16TFA sol. The intense anatase (101) peak is indicative of its high crystallinity compared to the low-temperature calcined samples. By contrast, even at 700 °C, the *control* and HOAc-modified TiO_2 samples were 100%
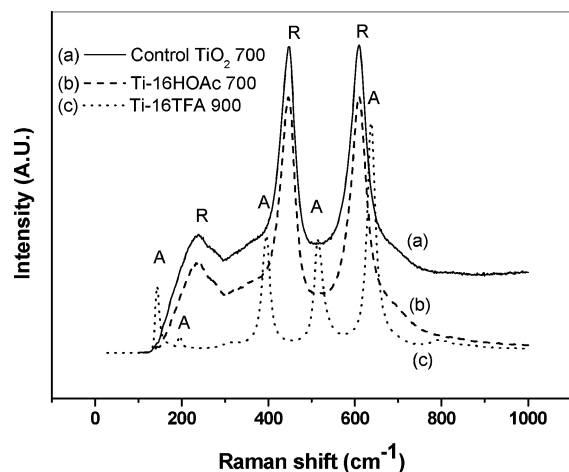
Figure 2. Raman spectra of (a) *control* TiO_2-700, (b) Ti-16HOAc-700, and (c) Ti-16TFA-900 (A, anatase; R, rutile) registered at 514 nm excitation wavelength.

197 rutile, while the OxA-modified TiO_2 showed a mixed phase
198 composition with 13% anatase and 87% rutile. For the
199 samples prepared with lower molar ratios of TFA, the
200 anatase-to-rutile transformation commences just below 700
201 °C for the Ti-1TFA sample (Figure 1a) and is completely
202 transformed to rutile at 900 °C. On the other hand, with the
203 Ti-8TFA sample, the conversion to rutile only starts at ca.
204 800 °C, and at 900 °C the sample contained ca. 57% rutile.
205 All the samples show a 100% rutile phase at 1000 °C
206 (Supporting Information 2).

207   Raman spectroscopy, being a more sensitive technique to
208 detect even traces of a compound, was also employed for
209 phase analysis (Figure 2). Ti-16TFA-500 (not shown here)
210 and Ti-16TFA-900 gave spectral bands corresponding to
211 anatase TiO_2 (144, 197, 395, 514, and 638 cm^{-1}).[21] The
212 *control* TiO_2 and Ti-16HOAc samples on the other hand were
213 converted to rutile at 700 °C (bands at 143, 233, 447, and
214 610 cm^{-1}).[22]

215   N_2 adsorption studies were conducted to examine the effect
216 of calcination on the textural properties. Ti-16TFA-900
217 showed a surface area of 20 $m^2 g^{-1}$ compared to that of the
218 *control* TiO_2 which was <1 $m^2 g^{-1}$ at 900 °C. The pore
219 radius measured using the Horvath−Kawazoe method indi-
220 cated the formation of a microporous network (9.273 Å) for
221 Ti-16TFA-900, while the *control* TiO_2-900 was almost
222 nonporous. The adsorption isotherm of Ti-16TFA-900 (Sup-
223 porting Information 3) also showed the presence of a
224 predominantly microporous network. The dramatic change
225 in the surface area and porosity values could be attributed
226 to the incorporation of F atoms. It is reported that F

227 incorporation into the silica network creates nanovoids.[23] The
228 evolution of microporosity in the present system is therefore
229 ascribed to a similar effect.

230   Diffuse reflectance spectral analyses were performed to
231 investigate the effect of calcination on the optical properties
232 of different powder samples (Supporting Information 4).
233 From such spectra, the band gap for the materials was
234 calculated. A band gap of 3.02 eV is obtained for the *control*
235 TiO_2-700 and -900 samples, which corroborate with the
236 reported data for rutile TiO_2.[2,5d] The Ti-16TFA-700 and -900
237 samples on the other hand showed a band gap of 3.28 eV.
238 Furthermore, a steady decrease in the percent reflectance in
239 the higher wavelength side of the spectrum demonstrates the
240 oxygen vacancy concentration of samples.[24] Such a sloping
241 baseline observed for Ti-16TFA-700 may be indicative of
242 the presence of oxygen vacancies. Ti-16TFA-900, on the
243 other hand, showed little change in baseline, consistent with
244 a sample relatively free of this defect (with minimal oxygen
245 vacancy).

246   To determine the role of TFA and especially whether any
247 fluorine can be observed after calcination, XPS has been
248 performed on the Ti-16TFA samples calcined at 500, 700,
249 800, 900, and 1000 °C. Figure 3a and b present the XPS
250 high-resolution spectra for F1s of Ti-16TFA-500 and Ti-
251 16TFA-900 samples, respectively. The photoelectron peak
252 located at 684.5 eV for Ti-16TFA-500 and Ti-16TFA-700
253 (Supporting Information 5) is ascribed to the F1s species of
254 F adsorbed on TiO_2.[25] Concentrations of 0.5 atom % F and
255 0.3 atom% F are determined for the Ti-16TFA-500 and Ti-
256 16TFA-700 samples, respectively. Similar peaks are however
257 absent in the Ti-16TFA-800 (Supporting Information 5) and
258 Ti-16TFA-900 samples. However the TGA pattern obtained
259 for the Ti-16TFA gel shows a small percent loss of mass up
260 to 800 °C. By contrast, the weight loss appeared to be
261 complete at ∼400 °C for the Ti-16HOAc and the *control*
262 TiO_2 gels (Supporting Information 6).

263   The presence of lattice F atoms is represented by a peak
264 located at 688 eV in XPS.[26] Such a peak could be observed
265 only for the Ti-16TFA-500 and Ti-16TFA-700 samples. XPS
266 is a surface technique whose analysis depth is 4−5 nm, and
267 therefore the presence of deep lattice F atoms (in Ti-16TFA-
268 800 and Ti-16TFA-900 samples, where the surface and near-
269 surface F atoms would be completely eliminated) may not
270 be observable using this technique. By contrast, FTIR should
271 be able to probe the presence of Ti−F bonds in the sample.
272 Figure 4 presents the FTIR spectra of the *control* TiO_2-500
273 and the various Ti-16TFA samples. A weak band at 1080
274 cm^{-1} is observed for the Ti-16TFA-500 sample, consistent
275 with the observation by Li et al. in the Mg−F system, but a
276 similar band could not be detected in any other samples, and

(21) (a) Music, S.; Gotic, M.; Ivanda, M.; Popovic, S.; Turkovic, A.; Trojko, R.; Sekulic, A.; Furic, K. *Mater. Sci. Eng., B* **1997**, *47*, 33. (b) Ivanda, M.; Music, S.; Popovic, S.; Gotic, M. *J. Mol. Struct.* **1999**, *480*, 645. (c) Huang, P. J.; Chang, H.; Yeh, C. T.; Tsai, C. W. *Thermochim. Acta* **1997**, *297*, 85. (d) Choi, H. C.; Jung, Y. M.; Kim, S. B. *Vib. Spectrosc.* **2005**, *37*, 33.

(22) (a) Pawlewicz, W. T.; Exarhos, G. J.; Conaway, W. E. *Appl. Optics* **1983**, *22*, 1837. (b) Peng, X.; Wang, J.; Thomas, D. F.; Chen, A. *Nanotechnology* **2005**, *16*, 2389. (c) Parker, J. C.; Segel, R. W. *Appl. Phys. Lett.* **1990**, *57*, 943. (d) Capwell, R. J.; Spagnolo, F.; De Sesa, M. A. *Appl. Spectrosc.* **1972**, *26*, 537. (e) Lei, Y.; Zhang, L. D.; Meng, G. W.; Li, G. H.; Zhang, X. Y.; Liang, C. H.; Chen, W.; Wang, S. X. *Appl. Phys. Lett.* **2001**, *78*, 1125. (f) Serpone, N.; Lawless, D.; Khairutdinov, R. *J. Phys. Chem.* **1995**, *99*, 16646.

(23) (a) Altshuler, S.; Chakk, Y.; Rozenblat, A.; Cohen, A. *Microelectron. Eng.* **2005**, *80*, 42. (b) Pankov, V.; Alonso, J. C.; Ortiz, A. *J. Appl. Phys.* **1999**, *86*, 275. (c) Kim, J.; Chung, J. C.; Sheen, D.; Sohn, Y. *J. Appl. Phys.* **2004**, *96*, 1435.

(24) Vratny, F.; Micale, F. *Trans. Faraday Soc.* **1963**, *59*, 2739.

(25) (a) Li, D.; Haneda, H.; Hishita, S.; Ohashi, N.; Labhsetwar, N. K. *J. Fluorine Chem.* **2005**, *126*, 69. (b) Park, H.; Choi, W. *J. Phys. Chem. B* **2004**, *108*, 4086.

(26) (a) Wang, Y. Q.; Sherwood, P. M. A. *Chem. Mater.* **2004**, *16*, 5427. (b) Yu, J. C.; Yu, J.; Ho, W.; Jiang, Z.; Zhang, L. *Chem. Mater.* **2002**, *14*, 3808.
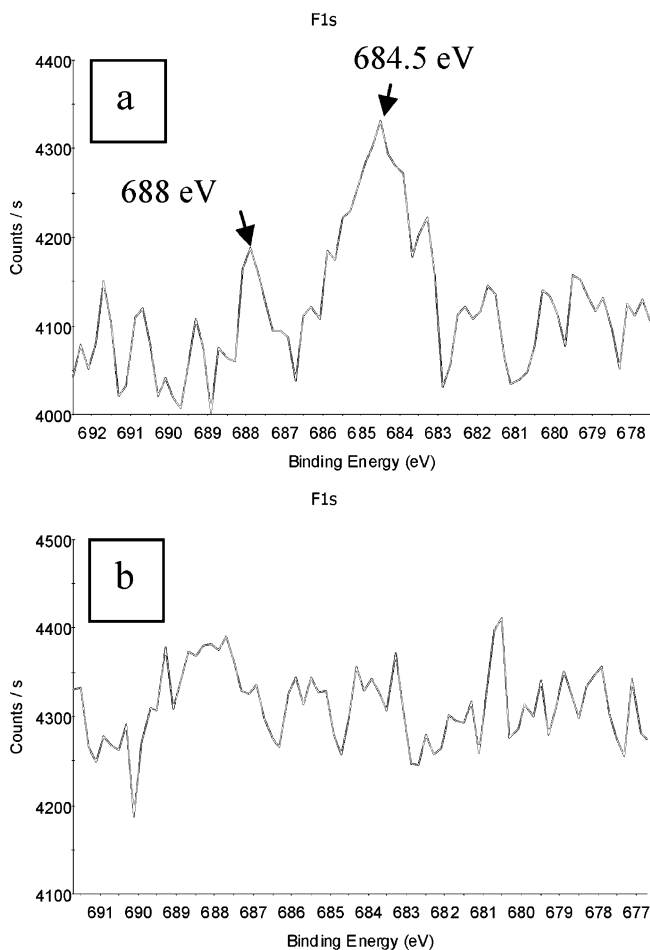
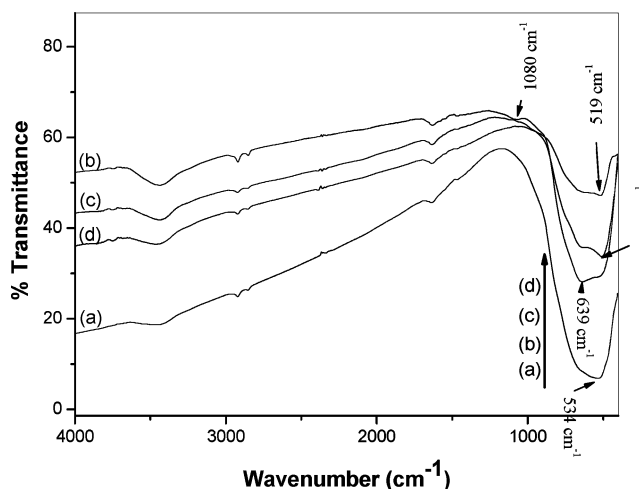**Figure 3.** XPS spectra of (a) Ti-16TFA-500 and (b) Ti-16TFA-900.

Figure 4. FTIR spectra of various TiO_2 samples [(a) *control* TiO_2-500, (b) Ti-16TFA-500, (c) Ti-16TFA-700, and (d) Ti-16TFA-900].

277 this may be attributed to the surface-fluorinated Ti−F
278 species.[27] Further, in the lower-wave-number region, a sharp
279 band centered at 534 cm^{-1} with a shoulder band at ∼648
280 cm^{-1} observed for the *control* TiO_2-500 represents the Ti−

281 O−Ti phonon vibration.[17a,27] In comparison, main bands at
282 639, 510, and 519 cm^{-1} can be observed for Ti-16TFA-500,
283 Ti-16TFA-700, and Ti-16TFA-900 samples, respectively.
284 The band at 639 cm^{-1} is ascribed to the surface Ti−F
285 bonds,[28] whereas the bands at 510 and 519 cm^{-1} are
286 consistent with a change in the chemical environment of the
287 titania matrix owing to the presence of a small amount of
288 lattice Ti−F bonds.[27b] The Ti-16TFA-800 sample showed a
289 similar pattern to Ti-16TFA-900 (Supporting Information 7).

290 In the sol−gel process, the hydrolysis (forced hydrolysis
291 in the present case) and polycondensation reactions occur
292 simultaneously as the sol was dried immediately after 24
293 hour aging. The drying process causes the formation of an
294 intimate gel of $Ti(OOCCF_3)_{4-x}(OH)_x$ (Supporting Information
295 1). The Ti−F bonds are only formed in the further condensa-
296 tion process (on calcination). This leads to the formation of
297 inlaid (deep) Ti−F bonds in the network structure. Those
298 Ti−F bonds, which are in the network structure, could not
299 be easily removed by heat treatment compared to the surface-
300 fluorinated ones. This explains the observations by TGA and
301 XPS. The mass loss shown by the Ti-16TFA gel up to 800
302 °C (above 400 °C) in TGA may be the mass loss of the
303 surface-fluorinated Ti−F species. The rest of the nominal
304 Ti−F bonds, which could not be quantified using XPS, may

(27) (a) Li, Z. *Thesis for doctor rerum naturalium (Dr. rer. nat.) im Fach Chemie*; Mathematisch-Naturwisenschaftlichen Fakultät Humboldt-Universität zu Berlin, Berlin, 2005. (b) Ignat'eva, L. N.; Polishchuk, S. A.; Antokhina, T. F.; Buznik, V. M. *Glass Phys. Chem.* **2004**, *30*, 139. (c) Osabe, D.; Seyama, H.; Maki, K. *Appl. Optics* **2001**, *41*, 739. (d) Scarel, G.; Aita, C. R.; Tanaka, H.; Hisano, K. *J. Non-Cryst. Solids* **2002**, *303*, 50.

(28) (a) Decken, A.; Nikiforov, G. B.; Passmore, J. *Dalton Trans.* **2006**, 4328. (b) Cavalli, M.; Gnappi, G.; Montenero, A.; Bersani, D.; Lottici, P. P.; Kaciulis, S.; Mattogno, G.; Fini, M. *J. Mater. Sci.* **2001**, *36*, 3253.

Table 2. Rate Constants of Various Degradation Reactions

sample	rate (min^{-1})
In UV light	
Degussa P25	0.327
control TiO_2-700	0.089
control TiO_2-900	0.021
Ti-12TFA-800	0.168
Ti-12TFA-900	0.200
Ti-32TFA-800	0.154
Ti-32TFA-900	0.246
Ti-16TFA-700	0.147
Ti-16TFA-800	0.197
Ti-16TFA-900	0.426
Ti-16HOAc-700	0.012
Ti-16OxA-700	0.028
In Sunlight	
Ti-16TFA-900	0.041
control TiO_2−700	0.006

be the inlaid ones. The influence of such Ti−F bonds could however be detected using FTIR.

Photoactivity. Kinetic plots of various methylene blue degradation experiments are presented in Figure 5. The corresponding rate constants are presented in Table 2. A complete degradation of MB was observed within 10 min under UV light irradiation for the Ti-16TFA-900 sample. By contrast, the *control* TiO_2-900, which was in a 100% rutile form, was found to be inactive up to a period of 6 h of UV irradiation. All the *control* samples took >2 h for complete methylene blue degradation. These results indicate that the TFA modification is highly effective in enhancing the photoactivity of TiO_2 at high temperatures. Furthermore, the activity for Ti-16TFA samples was in the order Ti-16TFA-900 > Ti-16TFA-800 > Ti-16TFA-700 > Ti-16TFA-600 > Ti16TFA-500. These observations demonstrate the significant role of anatase crystallinity, surface properties, and the minimal oxygen vacancy concentration
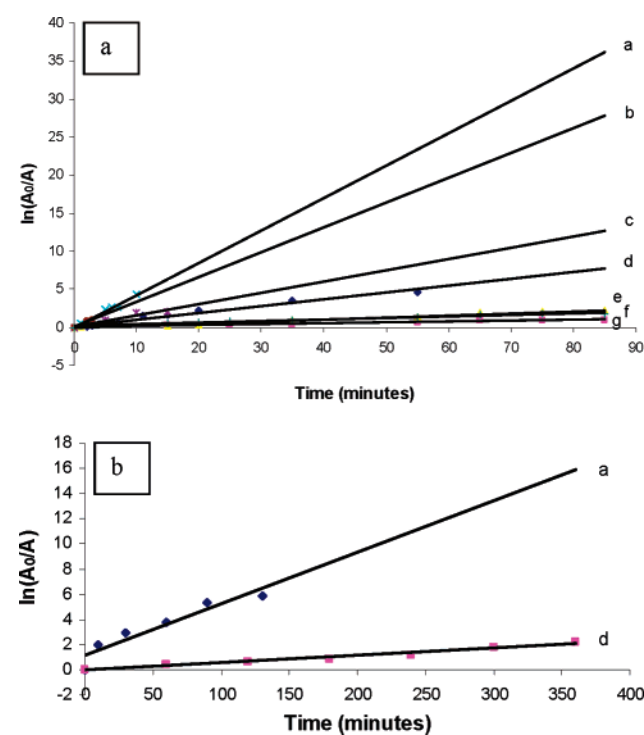

Figure 5. Methylene blue degradation kinetics of various TiO_2 samples in the presence of UV light (a) and sunlight (b) [(a) Ti-16TFA-900, (b) Degussa P25, (c) Ti-16TFA-700, (d) *control* TiO_2-700, (e) Ti-16OxA-700, (f) *control* TiO_2-900, and (g) Ti-16HOAc-700; A, absorbance at 664 nm].

on the photoactivity of TiO_2. Similar experiments have also been conducted in Dublin sunlight, where the Ti-16TFA-900 showed a complete degradation of MB in 90 min (Figure 5b). On the other hand, the *control* TiO_2-700 could not degrade MB even after 10 h of solar light irradiation (Supporting Information 8).

Discussion

Phase Evolution. Among the samples, Ti-16TFA-900 shows the highest anatase-to-rutile phase transformation temperature (900 °C) compared to the low TFA samples and the samples prepared with HOAc, OxA, and *control* TiO_2. An increase in the TFA concentration (Ti-32TFA), however, shows a similar effect on the phase transformation to that of Ti-16TFA. The structural evolution of the samples—phase formation and phase transformation—investigated by both Raman and XRD demonstrate the effect of different modifiers. The anatase-to-rutile transformation involves the rearrangement of the (TiO_6^{2-}) octahedron.[29] The structure of anatase consists of zigzag chains of octahedra, linked to each other through shared edges, whereas in rutile, a linear chain of opposite edge-shared octahedra is found. Chains are further linked to each other by sharing corner oxygen atoms to form a 3D network. In our case, the metal cation (Ti^{4+}) is expected to undergo a coordination expansion to six when chelated with TFA to form the independent Ti-$(OOCCF_3)_4$ octahedral complexes.[30] Further, when hydrolysis and condensation is initiated under the forced reaction conditions (temperature-dependent hydrolysis and condensation), initially, the independent octahedral complexes are hydrolyzed, forming $Ti(OOCCF_3)_{4-x}(OH)_x$ species. The next step is the condensation of two octahedral complexes to form the vertex-shared octahedra.[30] Upon further heating, the condensation between the two vertex-shared octahedra leads to the formation of an edge-shared octahedra, which is followed by the linking up of a third octahedron. The spatial factors offered by the trifluoroacetate complex may cause the joining up of a third octahedron to the far corner of the dioctahedra, thereby reducing the electrostatic repulsion.[31] Subsequently, when the temperature is sufficiently high, the decomposition of the trifluoroacetate complex occurs. The faster thermal decomposition (cleavage of Ti−$OOCCF_3$ bond) keeps up the rate of segregation (condensation), and under such a fast rate, the third octahedron will, preferentially, join to the existing dioctahedral complex to form a right-angled trioctahedral complex (anatase). This is perfectly in line with the previous reports, where it was suggested that the faster reaction rate promotes the formation of anatase rather than the thermodynamically favorable rutile structure.[32,33] The thermal

(29) (a) Matsumoto, Y.; Shono, T.; Hasegawa, T.; Fukumura, T.; Kawasaki, K.; Ahmet, P. *Science* **2001**, *291*, 854. (b) Garvie, R. C. *J. Phys. Chem.* **1978**, *82*, 218. (c) Shannon, R. D.; Pask, J. A. *Am. Mineral.* **1964**, *49*, 1707. (d) Depero, L. E.; Sangaletti, L.; Allieri, B.; Bontempi, E.; Marino, A.; Zocchi, M. *J. Cryst. Growth.* **1999**, *198/199*, 516. (e) Diebold, U. *Surf. Sci. Rep.* **2003**, *48*, 53.

(30) Livage, J.; Henry, M. In *Ultrastructure Processing of Advanced Ceramics*; Mackenzie, J. D.; Ulrich, D. R., Eds.; Wiley: New York, 1988; p 183.

(31) (a) Gopal, M.; Chan, W. J. M.; De Jonghe, L. C. *J. Mater. Sci.* **1997**, *32*, 6001. (b) Yin, H.; Wada, Y.; Kitamura, T.; Kambe, S.; Murasawa, S.; Mori, H.; Sakata, T.; Yanagida, S. *J. Mater. Chem.* **2001**, *11*, 1694. (c) Li, Y.; Lee, N. H.; Hwang, D. S.; Song, J. S.; Lee, E. G.; Kim, S. J. *Langmuir* **2004**, *20*, 10838.

(32) Yanagisawa, K.; Ovenstone, J. *J. Phys. Chem. B* **1999**, *103*, 7781.

Scheme 2. Schematic Representation of Anatase and Rutile Crystallization Events[a]
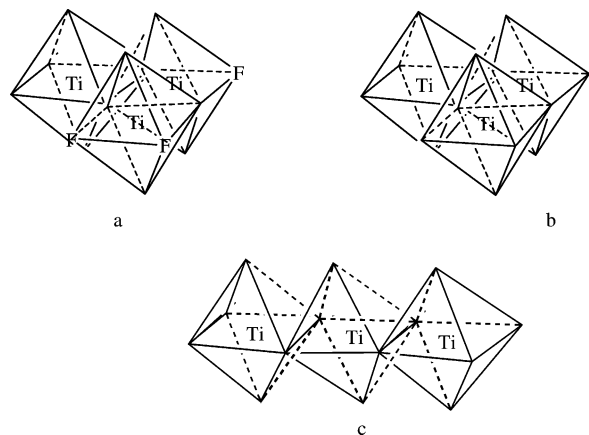
[a] (a) Anatase crystallization under the faster reaction conditions: the third octahedron, under the influence of fluorine, prefers to join to the existing dioctahedra by sharing an edge, forming a zigzag structure. (b) Anatase crystal structure after the removal of fluorine. (c) Rutile formation: the third octahedron preferably links up to the existing dioctahedra, forming a linear chain by sharing a pair of opposite edges, which is a thermodynamically favorable process. Under the high-temperature calcination process, the existing anatase clusters undergo a diffusional rearrangement to form the denser rutile crystals.

decomposition of trifluoroacetate species also causes the fluorination of the remaining amorphous precipitate as well as the existing anatase crystals (Scheme 2a). Under the fluorinated condition, the crystallization as well as the crystal growth can be a slow process due to the fact that the fluorinated clusters may repel each other, slowing down the reaction rate.[32] The inhibition of crystallization and crystal growth in such cases can be observed from the limitation of the X-ray peak intensity as well as the slower line-narrowing of the X-ray diffraction lines under the increasing calcination temperature. Upon further heating, the fluorine atoms are being preferentially eliminated (Scheme 2b), causing a faster atomic/ionic diffusion. Such faster diffusion conditions are favorable for the formation of a denser rutile structure (Scheme 2c).

The primary crystallite sizes calculated using the Scherrer equation showed crystallite sizes of 26, 32, 33, 34 and 35 nm respectively for the Ti-16TFA-500, Ti-16TFA-600, Ti-16TFA-700, Ti-16TFA-800, and Ti-12TFA-900 samples (Supporting Information 9). In addition, a direct dependence between the TFA concentration and rutile phase formation can be noticed. The rutile phase formation occurs when the anatase crystallite size was at 29, 31, 32, and 36 nm respectively for the Ti-1TFA, Ti-4TFA, Ti-8TFA, and Ti-12TFA samples, and for *control* TiO$_2$, it was at 26 nm. The shift in the phase transformation temperature with TFA addition can therefore be attributed to the presence of fluorine in the system. As the TFA concentration increases, there is a greater chance of the F atoms being trapped in the titania matrix. Upon further heating, fluorine is eliminated easily from the sample with low fluorine content, whereas the elimination could be very slow from the samples with high fluorine content, consistent with the high amount of deep-level trapped fluorine. As fluorine elimination and crystal growth are simultaneous events, the crystallites have a chance to grow to a greater extent in the high-TFA samples. Thus, the critical size limit for the phase transformation of the anatase crystals is shifted to higher crystallite size values for high-TFA samples in the present case. By contrast, the absence of fluorine in the *control* TiO$_2$ system caused a faster temperature-dependent diffusional rearrangement, after the initial anatase clustering, leading to the formation of a denser rutile structure at a comparatively lower temperature of 700 °C. Essentially, the fluorine substituted in the oxygen atomic site inhibits the extensive Ti−O−Ti bridging (Scheme 2a). These defect centers will also act as a barrier for oxygen ion diffusion necessary for the grain growth and assisted phase transformation.[34] This clearly suggests the inhibiting role of fluorine on the rutile phase nucleation, which may only be commenced after the elimination of F atoms from the structure. The higher bond enthalpy of Ti−O bonds (672 ± 9 kJ mol^{-1}) compared to the Ti−F bonds (569 ± 33 kJ mol^{-1}) may account for the preferential F elimination.[35]

It should be stated here that, even though the optimum amount of fluorine necessary for the inhibition of rutile phase nucleation cannot be calculated quantitatively, the present studies indicate that an initial concentration of 16 mol % TFA is sufficient to retain the anatase phase up to 900 °C. This is further ascertained from the fact that a higher TFA concentration (32 mol %) shows a similar effect as 16 mol % TFA and a lower concentration (12 mol %) could not prevent the phase transformation up to 900 °C. It should also be noted that a ±5% error can be expected in determining the phase content.

Photocatalytic Activity. MB degradation experiments and the corresponding kinetic analyses data show the highest activity for the Ti-16TFA-900 sample compared to the other TFA samples (both lower temperature and various concentration TFA samples) and those prepared with HOAc, OxA, and *control* TiO$_2$. Semiconductor photocatalytic reactions are known to occur through (i) direct valence band hole (h$_{VB}$) oxidation,[36] (ii) reactive oxygen species (namely, OH$^{\bullet}$, O^{2-}, and H$_2$O$_2$)[36−37] assisted oxidation, and (iii) direct conduction band electron (e$_{CB}$) reduction. The enhanced photocatalytic activity[36,38] and photoinduced hydrophilicity[39] of surface-fluorinated TiO$_2$ systems have been reported recently.

(33) Meakin, P. In *Kinetics of aggregation and gelation*; Family, F.; Landau, D. P., Eds.; North Holland Physics Publishing: New York, 1984; p 91.

(34) (a) Ding, D.; Liu, X. *J. Mater. Res.* **1998**, *19*, 2556. (b) Rao, C. N.; Rao, R. J. *Phase transitions in solids*; McGraw Hill: New York, 1978; p 82. (c) Zhang, H.; Banfield, J. F. *J. Mater. Res.* **2000**, *15*, 437.
(35) Lide, D. R. *CRC Handbook of Physics and Chemistry*, 84th ed.; CRC: Boca Raton, FL, 2003.
(36) (a) Maurino, V.; Minero, C.; Mariella, G.; Pelizzetti, E. *Chem. Commun.* **2005**, 2627. (b) Minero, C.; Mariella, G.; Maurino, V.; Pelizzetti, E. *Langmuir* **2000**, *16*, 2632. (c) Minero, C.; Mariella, G.; Maurino, V.; Vione, D.; Pelizzetti, E. *Langmuir* **2000**, *16*, 8964.
(37) (a) Goto, H.; Hanada, Y.; Ohno, T.; Matsumura, M. *J. Catal.* **2004**, *225*, 223. (b) Cermenati, L.; Pichat, P.; Guillard, C.; Albini, A. *J. Phys. Chem. B* **1997**, *101*, 2650. (c) Kormann, C.; Bahnemann, D. W.; Hoffmann, M. R. *Environ. Sci. Technol.* **1988**, *22*, 798. (d) Hykaway, N.; Sears, W. M.; Morisaki, H.; Morrison, S. R. *J. Phys. Chem.* **1986**, *90*, 6663. (e) Morrison, S. R. *Electrochemistry at Semiconductor and Oxidized Metal Electrodes*; Plenum Press: New York, 1980; p 257. (f) Cai, R.; Kubota, Y.; Fujishima, A. *J. Catal.* **2003**, *219*, 214.
(38) (a) Wang, R.; Hashimoto, K.; Fujishima, A.; Chikuni, M.; Kojima, E.; Kitamura, A.; Shimohigoshi, M.; Watanabe, T. *Nature* **1997**, *388*, 431. (b) Tang, J.; Quan, H.; Ye, J. *Chem. Mater.* **2007**, *19*, 116.

Recently, Maurio et al. reported that the fluorinated TiO$_2$ systems increase the generation of adsorbed and free OH$^\bullet$ radicals.[39] Such an enrichment in the reactive species concentration in suspension was associated with a considerable enhancement in the photocatalytic activity.[39] In addition, F doping was also found to enhance the photocatalytic activity of TiO$_2$.[25a,40] Despite many studies, the exact mechanism of the photocatalytic reaction and the role of influencing parameters in such systems is still not clear. The influence of F atoms in different systems is reported differently.[25a,39,40] The present sol–gel method enabled the preparation of both surface-fluorinated and F-doped TiO$_2$ systems from a single process, allowing a direct and straightforward comparison of their activity. High-temperature heat treatment (900 °C) enabled the preparation of F-doped TiO$_2$ (small amount of F) with high crystallinity and microporosity, whereas the low-temperature heat treatment (500–700 °C) produced surface-fluorinated TiO$_2$. The Ti-16TFA-900 sample showed a higher photocatalytic activity compared to the surface-fluorinated TiO$_2$ in the present study.

The photocatalytic activity of titania is mainly dependent on factors such as accessible surface area, crystallinity, and particle size.[41] The microporous nature of Ti-16TFA-900 increases the accessibility of MB molecules to have maximum surface coverage by direct adsorption, which effectively enhances its reaction efficiency.[25b] The lower activity of the low-temperature Ti-16TFA samples (activities in the order Ti-16TFA-500 < Ti-16TFA-600 < Ti-16TFA-700 < Ti-16TFA-800 < Ti-16TFA-900), in comparison, despite their high surface accessibility (high surface areas), is ascribed to the high electronegativity of fluorine, which inhibits the interfacial charge transfer. In other words, the steady increase in activity with an increase in calcination temperature up to 900 °C may be attributed to the gradual elimination of the fluorine incorporated in the titania matrix. In addition, fluorine when incorporated into the titania matrix increases the oxygen vacancy concentration. Subbarao et al. reported the facilitating effect of oxygen vacancy on charge carrier recombination.[42] The present observations are consistent with the report by Subbarao et al., where the high photoactivity is obtained for the sample with a high crystallinity, microporosity, and minimal oxygen vacancy concentration. The hydroxyl-radical-generating ability of the F

atoms,[39] in the case of the low-temperature samples, has been nullified by the increase in oxygen vacancies. Therefore, the presence of fluorine can be assumed to be detrimental to the activity as it (i) reduces the rate of interfacial charge transfer and (ii) creates more oxygen vacancies.

Three factors have been identified which enhance the activity of the Ti-16TFA-900 sample compared to the surface-fluorinated TiO$_2$ samples in the present study. First is the high anatase crystallinity of Ti-16TFA-900 compared to the low-temperature calcined samples. Second is the presence of minimal F content (minimal oxygen vacancy) that reduces the charge carrier recombination process in Ti-16TFA-900 compared to the low-temperature calcined Ti-16TFA samples. The presence of these nominal inlaid F atoms increases the surface −OH groups, adsorbed OH$^\bullet$ radicals, and free OH$^\bullet$ radicals (in solution). In case of the low-temperature Ti-16TFA samples, the higher electronegativity of the surface-fluorinated F atoms will have more influence in reducing the interfacial charge transfer compared to the generation of such reactive species. The relatively high adsorbing ability of surface F atoms (water and organic adsorption, especially MB) in such systems is nullified by the poor interfacial charge transfer to the adsorbed molecules. Finally, this material shows far more suitable surface properties, that is, a microporous nature of the Ti-16TFA-900 sample with an enhanced probability of interfacial charge transfer. Despite having high surface area values, the low-temperature Ti-16TFA samples are less active due to the factors described above. The hindering effect on rutile phase nucleation by fluorine up to a temperature as high as 900 °C was therefore helpful in attaining a highly crystalline and microporous anatase TiO$_2$. The high photoactivity of the Ti-16TFA-900 sample is therefore ascribed to the synergistic effect of high crystallinity, microporosity, and minimum oxygen vacancy concentration, which could well be achieved by the high-temperature heat treatment. On the other hand, the *control* TiO$_2$ samples are in the pure rutile form with low porosity at these temperatures (700 and 900 °C) and are therefore less active. It should be noted here that the red-shifting of the band gap absorption of *control* TiO$_2$ samples, which could have been favorable for the photoactivity, has been nullified by the nonporous and noncatalytic nature of the rutile phase.

Summary

In summary, a simple and highly efficient procedure for the preparation of high-temperature stable anatase (100% at 900 °C) titania with a high photocatalytic activity is presented. Fluorine-assisted inhibition of rutile phase nucleation followed by the elimination of fluorine and subsequent commencement of rutile phase nucleation explains the high-temperature stability for the Ti-16TFA samples. The Ti-16TFA-900 sample shows the highest photocatalytic activity in the presence of both UV light (λ 365 nm) and sunlight, which is attributed to a synergistic effect of the high crystallinity, microporosity, and a minimal oxygen vacancy concentration of anatase TiO$_2$. This intrinsic doping approach is therefore proposed to be an effective methodology for replacing the conventional use of extrinsic cationic dopants to obtain a high-temperature stable anatase phase. The present sol–gel process to produce highly crystalline

(39) (a) Yu, J. C.; Ho, W.; Yu, J.; Hark, S. K.; Iu, K. *Langmuir* **2003**, *19*, 3889. (b) Hattori, A.; Yamamoto, M.; Tada, H.; Ito, S. *Chem. Lett.* **1998**, 707. (c) Hattori, A.; Shimota, K.; Tada, H.; Ito, S. *Langmuir* **1999**, *15*, 5422. (d) Yamaki, T.; Sumita, T.; Yamamoto, S. *J. Mater. Sci. Lett.* **2002**, *21*, 33. (e) Fujihara, S.; Kusakado, J.; Kimura, T. *J. Mater. Sci. Lett.* **1998**, *17*, 781.

(40) (a) Wang, J.; Yin, S.; Zhang, Q.; Saito, F. *J. Mater. Chem.* **2003**, *13*, 2348. (b) Yamaki, T.; Umebayashi, T.; Sumita, T.; Yamamoto, S.; Maekawa, M.; Kawasuso, A.; Itoh, H. *Nucl. Instrum. Methods Phys. Res., Sect. B* **2003**, *206*, 254. (c) Ayllon, J. A.; Peiro, A. M.; Saadoun, L.; Vigil, E.; Domenech, X.; Peral, J. *J. Mater. Chem.* **2000**, *10*, 1911. (d) Vohra, M. S.; Kim, S.; Choi, W. *J. Photochem. Photobiol., A* **2003**, *160*, 55.

(41) (a) Harada, H.; Ueda, T. *Chem. Phys. Lett.* **1984**, *106*, 229. (b) Nishimoto, S. I.; Ohtani, B.; Kajiwara, H.; Kagiya, T. *J. Chem. Soc., Faraday Trans.* **1985**, *1*, 61. (c) Bickley, R. I.; Carreno, T. G.; Lees, J. S.; Palmisano, L.; Tilley, R. J. D. *J. Solid State Chem.* **1991**, *92*, 178. (d) Xu, N.; Shi, Z.; Fan, Y.; Dong, J.; Shi, J.; Hu, M. Z.-C. *Ind. Eng. Chem. Res.* **1999**, *38*, 373.

(42) Subbarao, S. N.; Yun, Y. H.; Kershaw, R.; Dwight, K.; Wold, A. *Inorg. Chem.* **1979**, *18*, 488.

anatase TiO_2 stable up to a temperature as high as 900 °C therefore has fundamental as well as technological importance.

Abbreviations. TTIP, titanium tetraisopropoxide; TFA, trifluoroacetic acid; HOAc, acetic acid; OxA, oxalic acid; MB, methylene blue.

Supporting Information Available: FTIR data showing the chelation of TFA (Supporting Information 1), XRD patterns of Ti-12TFA and Ti-32TFA samples calcined at 900 °C (Supporting Information 2), N_2 adsorption and desorption isotherms of a Ti-16TFA-900 sample (Supporting Information 3), diffuse reflectance spectra (Supporting Information 4), high-resolution XPS spectra of Ti-TFA-800 and Ti-16TFA-900 (Supporting Information 5), TGA analysis graphs (Supporting Information 6), FTIR spectra (Supporting Information 7), extensive UV−vis spectral characterization data (Supporting Information 8), and a table showing the crystallite sizes of samples (Supporting Information 9). This material is available free of charge via the Internet at http://pubs.acs.org.